Impedance Based Analysis of DFIG Stator Current Unbalance and Distortion Suppression Strategies

Song, Yipeng; Zhou, Dao; Blaabjerg, Frede

Published in:
Proceedings of the 42nd Annual Conference of IEEE Industrial Electronics Society, IECON 2016

DOI (link to publication from Publisher):
10.1109/IECON.2016.7793220

Publication date:
2016

Impedance Based Analysis of DFIG Stator Current Unbalance and Distortion Suppression Strategies

Yipeng Song, Dao Zhou, Frede Blaabjerg
Department of Energy Technology, Aalborg University
Aalborg 9220, Denmark
yis@et.aau.dk, zda@et.aau.dk, fbl@et.aau.dk

***Abstract* — The control strategies of Doubly Fed Induction Generator (DFIG) system output current unbalance and distortion suppression have been well investigated in detail, with the implementation of two kinds of resonant regulators, i.e., conventional Resonance (R) regulator or Vector Proportional Integral (VPI) regulator. Nevertheless, these two resonance regulators have never been compared from the perspective of suppression capability of output current unbalance and distortion. In this paper, the impedance based analysis method is adopted to theoretically explain and compare the DFIG system impedance reshaping though the introduction of R and VPI regulator. It is pointed out that, when implemented in the DFIG system output current unbalance and distortion suppression, the VPI regulator (equivalent to the combination of virtual positive inductor and virtual positive resistor) has two advantages over R regulator (equivalent to the combination of virtual positive resistor and virtual negative inductor), i.e., better high order harmonic distortion suppression. The theoretical analysis and MATLAB simulation results have validated the correctness of this conclusion.**

Keywords—DFIG system impedance; unbalance and distortion; R regulator and VPI regulator; virtual impedance.

I. INTRODUCTION

The Doubly Fed Induction Generator (DFIG) based wind power generation system, which has been a major focus of renewable power generation for the past decades, are becoming more and more popular in the worldwide. Due to the direct connection of DFIG stator winding to the power grid, the DFIG system is quite vulnerable to the grid network voltage unbalance and harmonic distortion at the Point of Common Coupling (PCC), and the detrimental performance will occur as a consequence, e.g., DFIG system overall output current unbalance and harmonic distortion, output active and reactive power pulsation, electromagnetic torque pulsation, dc-link voltage fluctuation and etc [1]-[7].

A large number of efforts have been done to improve the DFIG system performance under these adverse grid network conditions [1]-[7]. Refs. [1]-[5] proposed the improved rotor current control strategy to ensure sinusoidal stator output current by calculating the rotor current harmonic components reference, in the other words, the achievement of sinusoidal stator output current is achieved by the indirect control of rotor current harmonic components.

On the other hand, Refs. [6]-[7] proposed the stator current direct control using conventional resonant regulator, in other words, besides the rotor current fundamental component closed-loop control responsible for outputting the harvested wind power, the direct closed-loop control of stator current based on resonant regulator is responsible for the output stator current harmonic distortion elimination. The advantages of this strategy are, no stator voltage negative and harmonic components extraction is needed, and the current control reference calculation is not required, which help to simplify the control structure.

The two different resonant regulators, i.e., conventional Resonant (R) regulator and Vector Proportional Integral (VPI) regulator, are often employed in [1]-[7]. Both these regulators are capable of providing sufficiently large magnitude at the selected resonant frequency 100Hz, 300Hz, 600Hz and 900Hz for the purpose of suppressing negative and harmonic components. However, these two resonant regulators have different phase response due to the different numerator expression, that is, first-order expression in R regulator and second-order expression in VPI regulator. The implementation of R regulator is equivalent to insert the combination of virtual positive resistor and negative inductor due to the inevitable digital control delay [8]. On the other hand, the employment of VPI regulator is equivalent to insert the combination of virtual positive resistor and positive inductor also due to the digital control delay. The detailed analysis of this difference will be conducted in Section II from the perspective of virtual impedance.

The impedance modeling analysis of DFIG system has been thoroughly investigated in [9]-[16], where the impedance modeling of rotor side converter (RSC) and DFIG machine, GSC and L filter are built up for the sub-synchronous resonance. In this paper, the DFIG system impedance modeling in [9]-[16] is used to analyze the output current unbalance and distortion suppression capability when R and VPI regulators are implemented in Section III.

This paper is organized as follows, the existing improved DFIG system output current control strategy is first reviewed in Section II as a foundation for the following discussion. The impedance of DFIG system considering the introduction of the improved current control strategy is built, and the different impedance shape caused by R and VPI regulator are compared in Section III. The simulation validation results are provided in Section IV based on 7.5 kW DFIG system simulation model. Finally, the conclusions are given in Section V.

978-1-5090-3474-1/16/$31.00 ©2016 IEEE

II. Existing DFIG System Improved Current Control Strategy and Impedance Modeling

For the purpose of delivering wind power with acceptable energy quality under unbalanced and harmonic distorted grid voltage, the improved DFIG system output current control strategies have been completely investigated, which are based on rotor current reference calculation and regulation in RSC [1]-[5], or based on stator current direct regulation in RSC [6]-[7], and grid side converter current regulation in GSC. In this section, these previous works are summarized to be the foundation of following discussions.

The control block diagram of the existing indirect rotor current control and direct stator current control in DFIG system can be summarized in Fig. 1. For the average power control in RSC and GSC, the rotor current fundamental component $\boldsymbol{I}^{+}_{rdq+}$ can be well regulated by PI regulator to deliver average wind power to the grid; the grid side current fundamental component $\boldsymbol{I}^{+}_{gdq+}$ can also be similarly regulated by PI regulator to keep constant dc-link voltage.

For the improved unbalance and distortion control in RSC and GSC, it should be noted that, for the GSC control, the grid side current can be directly regulated, while the main difference occurs in the RSC control strategy, i.e., the indirect rotor current control, and direct stator current control in RSC as illustrated below.

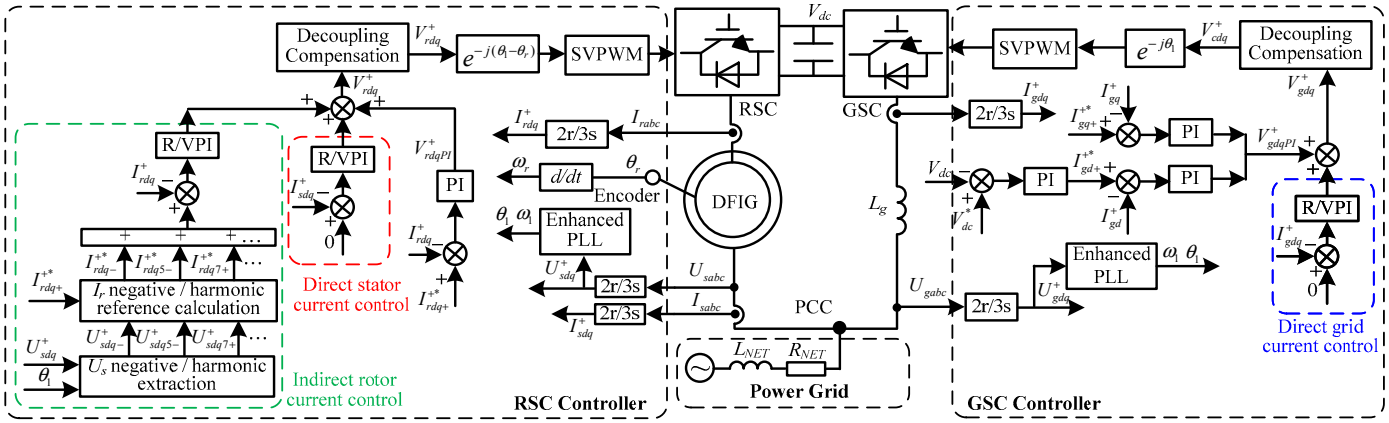

Fig. 1. Control block diagram of the existing indirect rotor current control / direct stator current control in DFIG system

A. Indirect rotor current and direct stator current control

For the indirect rotor current control, the stator voltage negative and harmonic components need first to be extracted, then the rotor current negative and harmonic components references need to be calculated. The actual rotor current can be accurately regulated by the R or VPI regulator to achieve the sinusoidal stator output current.

For the direct stator current control, the stator current is directly regarded as the control feedback, and the control reference is set to zero, thus the stator current can be directly regulated by R or VPI regulator. The advantage of this control strategy is that no stator voltage negative and harmonic extraction is required, and no reference calculation is need.

B. R and VPI regulator

The R regulator [1]-[5] can be expressed as,

$$C_R(s)=\frac{k_r\omega_c s}{s^2+\omega_c s+(n\omega_1)^2} \tag{1}$$

where, k_r is the regulator resonant parameter, ω_c is the resonant bandwidth parameter, ω_1 is the fundamental component angular speed of 100π rad/s, n can be assigned with 2 for negative components regulation, or 6, 12, 18… for the harmonic components regulation.

The VPI regulator [7] can be expressed as,

$$C_{VPI}(s)=\frac{\left(k_{pr}s+k_{ir}\right)\omega_c s}{s^2+\omega_c s+(n\omega_1)^2} \tag{2}$$

where, k_{pr} and k_{ir} are the regulator proportional and integral parameters which need to satisfy the rule of pole-zero cancellation [7].

As shown in Fig. 2, both regulators are capable of providing sufficiently large magnitude response around 40dB at the tuned resonant frequency, thus the satisfactory suppression of output current negative and harmonic components can be ensured. The difference can only be observed in their phase response, i.e., the phase response at the resonant frequency is 90° for VPI regulator, and 0° for the R regulator. This phase difference will be further explained from the perspective of virtual impedance.

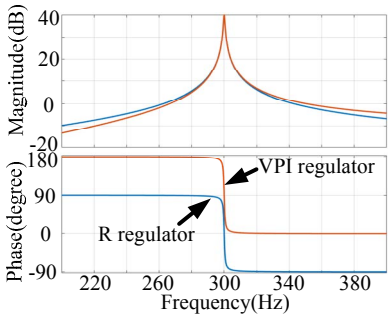

Fig. 2. Bode diagram of R and VPI regulator, k_r = 100, k_{pr} = 0.053, k_{ir}=1, ω_c=5 rad/s, n=6, ω_1 = 100π rad/s

C. Impedance modeling of R and VPI regulator concerning digital control delay

Importantly, the digital control delay is always inevitable in the DFIG system control strategy, typically one and half the sample period [8], thus it can be presented as,

$$G_d(s)=e^{-sT_d} \tag{3}$$

where, control delay of T_d is $1.5T_s$, T_s is the sample period.

According to (1), it can be found out that the R regulator can be regarded as the combination of a resonant regulator with unity magnitude response at the resonant frequency and a positive resistor k_r, as shown below.

$$C_R(s)=\underset{\substack{\uparrow\\ \text{positive}\\ \text{resistor}}}{k_r}\frac{\omega_c s}{s^2+\omega_c s+(n\omega_1)^2}\quad\begin{matrix}\uparrow\\ \text{unity magnitude}\\ \text{resonant regulator}\end{matrix} \tag{4}$$

Based on (3) and (4), the positive resistor introduced by R regulator can be transformed to the combination of positive resistor and negative inductor as following,

$$k_r e^{-sT_d}=k_r\cos(n\omega_1 T_d)-jk_r\sin(n\omega_1 T_d) \tag{5}$$

Similarly, the VPI regulator can be regarded as the combination of unity magnitude response resonant regulator at the resonant frequency and the positive resistor k_{ir} + positive inductor k_{pr} as shown below.

$$C_{VPI}(s)=\underset{\substack{\uparrow\\ \text{positive resistor}+\\ \text{positive inductor}}}{(k_{pr}s+k_{ir})}\frac{\omega_c s}{s^2+\omega_c s+(n\omega_1)^2}\approx\underset{\substack{\uparrow\\ \text{positive inductor}}}{k_{pr}s}\frac{\omega_c s}{s^2+\omega_c s+(n\omega_1)^2}\quad\begin{matrix}\uparrow\\ \text{unity magnitude}\\ \text{resonant regulator}\end{matrix} \tag{6}$$

Note that the pole-zero cancellation rule requires that $k_{pr}/k_{ir} = \sigma L_r/R_r$ [7], where σ is the leakage inductance coefficient, L_r is the rotor inductance, R_r is the rotor resistance. Moreover, since the unbalanced and distorted grid frequencies discussed in this paper are 100 Hz, 300 Hz, 600 Hz and 900 Hz respectively, thus the value of $k_{pr}s$ is much larger than the value of k_{ir}. As a result, the positive resistor k_{ir} part can be neglected, and the virtual positive inductor $k_{pr}s$ part can be introduced via the VPI regulator.

Similarly, based on (3) and (6), due to the digital control delay, the positive inductor introduced by VPI regulator can be transformed to the combination of positive inductor and positive resistor as following,

$$k_{pr}se^{-sT_d}=jn\omega_1 k_{pr}\cos(n\omega_1 T_d)+k_{pr}n\omega_1\sin(n\omega_1 T_d) \tag{7}$$

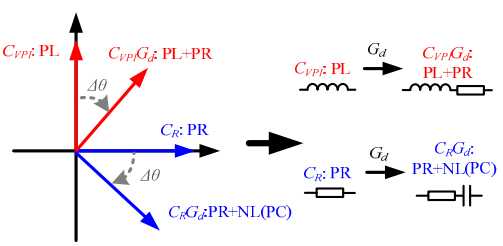

Fig. 3. Vector diagram of the virtual impedance with and without the consideration of digital control delay when R and VPI regulator is enabled

Fig. 3 gives out the vector diagram of the virtual impedance with and without the consideration of digital control delay. As it can be seen, the digital control delay causes the rotation of impedance vector clockwise, and the rotating angle $\Delta\theta$ is the same regardless of which regulator is employed, it is determined by the control delay time and the control harmonic frequency as following,

$$\Delta\theta=n\omega_1 T_d\frac{180}{\pi} \tag{8}$$

Thus, based on (8), the rotating angle of virtual positive inductor introduced by VPI or positive resistor by R regulator can be presented in Table I, $T_d = 1.5T_s$ = 1.5e-4 s.

TABLE I. ROTATING ANGLE OF VIRTUAL IMPEDANCE

Components	n	$\Delta\theta$
Negative	2	5.4 °
5th 7th harmonic	6	16.2 °
11th 13th harmonic	12	32.4 °
17th 19th harmonic	18	48.6 °

It is obvious that as the control frequency increases, the rotating angle $\Delta\theta$ caused by the digital control delay becomes larger. This indicates that, for the VPI regulator, the magnitude of virtual resistance becomes larger, and the magnitude of virtual inductor becomes smaller; while for the R regulator, the magnitude of virtual resistance becomes smaller, while the virtual negative inductance becomes larger. Importantly, since both impedance of DFIG machine and RSC as well as GSC and L filter behave as inductive units, the virtual negative inductance will unfortunately result in the magnitude decreasing, which results in the deterioration of DFIG system unbalance and distortion suppression. This influence is more severe for the higher harmonic distortion suppression, and it will be illustrated in following discussion.

D. DFIG system impedance modeling

Clearly, the two different kinds of improved control strategies in RSC, i.e., indirect rotor current control and direct stator current control, give out two different impedance modeling results. Fig. 4 gives out the impedance modeling of RSC and DFIG machine with (a) indirect rotor current control, (b) direct stator current control, both R and VPI regulators can be implemented in the two control strategies. Also, it should be pointed out that, unlike the impedance modeling built up in the stationary reference frame in [13], the impedance modeling in this paper is built in the *dq* synchronous reference frame, thus no frequency shifting of 50 Hz and slip angular speed need to be taken into consideration.

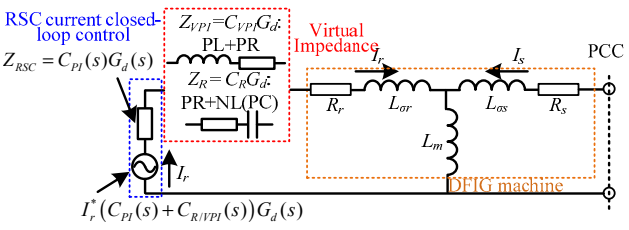

(a) indirect rotor current control

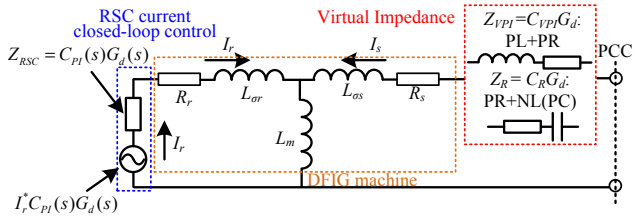

(b) direct stator current control

Fig. 4. Impedance modeling of RSC and DFIG machine with (a) indirect rotor current control, (b) direct stator current control

Therefore, based on Fig. 4(a), the impedance of RSC and DFIG machine with indirect rotor current in the *dq* synchronous reference frame can be presented as,

$$Z_{R\_R/VPI}=\frac{Z_{Lm}H+(R_s+Z_{L\sigma s})H+Z_{Lm}(R_s+Z_{L\sigma s})}{Z_{Lm}+H} \quad (9)$$

where, the first subscripts "*R*" and "*S*" indicate the indirect rotor current control and direct stator current control, the second subscripts "*R*" and "*VPI*" indicate the R and VPI regulator. $H = R_r + Z_{L\sigma r} + Z_{RSC} + Z_{R/VPI}$; $Z_{RSC} = C_{PI}(s)G_d(s)$; $Z_{R/VPI} = C_{R/VPI}(s)G_d(s)$; $Z_{Lm} = sL_m$ is mutual inductance; $Z_{L\sigma r} = sL_{\sigma r}$ is rotor leakage inductance, $Z_{L\sigma s} = sL_{\sigma s}$ is stator leakage inductance, R_s is the stator resistance.

Similarly, based on Fig. 4(b), the impedance of RSC and DFIG machine with direct stator current can be presented as,

$$Z_{S\_R/VPI}=\frac{Z_{Lm}J+(R_s+Z_{L\sigma s}+Z_{R/VPI})J+Z_{Lm}(R_s+Z_{L\sigma s}+Z_{R/VPI})}{Z_{Lm}+J} \quad (10)$$

where, $J = R_r + Z_{L\sigma r} + Z_{RSC}$, R_r is the rotor resistance.

According to Fig. 1, the GSC and L filter impedance modeling can be obtained as shown in Fig. 5.

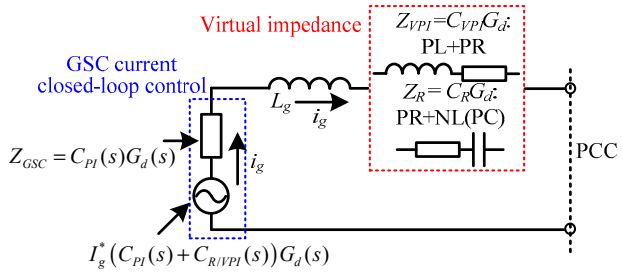

Fig. 5. Impedance modeling of GSC and L filter

Therefore, based on Fig. 5, the impedance modeling of GSC and L filter can be obtained as,

$$Z_{G\_R/VPI}=Z_{GSC}+Z_{Lg}+Z_{R/VPI} \quad (11)$$

where, $Z_{GSC} = C_{PI}(s)G_d(s)$, $Z_{R/VPI} = C_{R/VPI}(s)G_d(s)$, $Z_{Lg} = sL_g$ is the output inductor filter inductance.

III. Unbalance and Distortion Suppression Capability of R and VPI Regulator

This section discusses the DFIG system impedance modeling with the introduction of the improved DFIG stator output current unbalance and distortion suppression with indirect rotor or direct stator current control using R and VPI regulator

A. Stator and grid current unbalance and distortion suppression using R and VPI regulator

Based on (9) and (10), Fig. 6 shows the Bode diagram of DFIG and RSC impedance for output stator current unbalance and distortion suppression, using indirect rotor current control and direct stator current control, with R and VPI regulator, k_r = 50, ω_c=5 rad/s, ω_0=100π rad/s. Z_{SR0} indicates that the improved control strategy is disabled as,

$$Z_{SR0}=\frac{Z_{Lm}H_0+(R_s+Z_{L\sigma s})H_0+Z_{Lm}(R_s+Z_{L\sigma s})}{Z_{Lm}+H_0} \quad (12)$$

where, $H_0 = R_r + Z_{L\sigma r} + Z_{RSC}$.

Fig. 6(a) shows the unbalance suppression circumstance, once either improved control strategy is enabled, the much higher magnitude response of direct stator current control can be obtained, i.e., from 17 dB to 35 dB at 100 Hz for Z_{S_R} and Z_{S_VPI}. While, the magnitude increasing extent is smaller for the indirect rotor current control, i.e., from 17 dB to 31.9 dB for Z_{R_R}, and from 17 dB to 29 dB for Z_{R_VPI}. From another point of view, it can also be found that, since the rotating angle $\Delta\theta$ = 5.4° for the 100 Hz control frequency is small enough to be neglected, both R and VPI regulators still acts as positive resistance and positive inductance, thus successfully implementing the output current unbalance suppression.

Fig. 6(b) shows the circumstance of low order 5th and 7th suppression in DFIG stator output current. Similar as the case of Fig. 6(a), since the rotating angle of 16.2° is still acceptably small, both R and VPI regulators still behaves as positive resistance and positive inductance to suppress the low order harmonic components. However, the magnitude dent at frequency higher than 300 Hz can be observed which is different from Fig. 6(a). Since the virtual negative inductance caused by the control delay in R regulator is equivalent to positive capacitance, this positive capacitance causes the magnitude dent due to the resonance between DFIG machine stator/rotor leakage inductance and the virtual positive capacitance. In contrast, magnitude response with the VPI regulator remains satisfactory without dent since the introduced virtual resistance is also helpful to increase the magnitude response at 300 Hz.

Fig. 6(c) shows the circumstance of 11th and 13th high order distortion suppression in DFIG stator output current. Obvious difference can be observed when R regulator or VPI regulator is implemented. Since the digital control delay causes large rotating angle of 32.4° at 600 Hz, the introduced virtual negative inductance in R regulator has a clear detrimental influence on the distortion suppression by small increasing of magnitude response from 29.4 dB to 33.9 dB at

600 Hz. Besides, the magnitude dent becomes much larger than the case of Fig. 6(b) due to the larger virtual negative inductance. In comparison, the magnitude response with the VPI regulator is much more satisfactory, i.e., from 29.4 dB to 37.8 dB, which guarantees the satisfactory suppression of 11th and 13th harmonic distortion.

Fig. 6(d) shows the circumstance of 17th and 19th high order distortion suppression in DFIG stator output current. As the worst case, the control delay causes the rotating angle of 48.6°, as a consequence, no magnitude increasing can be produced when the R regulator is employed due to the large virtual negative inductance, instead a large dent is unfortunately produced. This means that, the R regulator fails to suppress the stator output current 17th and 19th distorted components due to the large virtual negative inductance cause by the digital control delay. In comparison, when the VPI regulator is introduced, the magnitude response increases from 32.9 dB to 38.8 dB since the virtual resistance and the positive inductance caused by the control delay are still beneficial to increase the magnitude response and mitigate the output stator current distortion at 900Hz.

Thus, based on above explanation, it can be concluded that, 1) due to the virtual negative inductance introduced by digital control delay, the unbalance and distortion suppression capability of R regulator becomes worse and even fails as the control frequency increases; 2) in contrast, the VPI regulator is capable of maintaining satisfactory suppression performance for both unbalance and distortion components since the virtual positive resistance is also helpful to mitigate the stator current negative and harmonic components; 3) the proposed indirect rotor current control strategy and direct stator current control strategy do not have obvious difference on the suppression performance, and the main difference of suppression performance attributes to the R or VPI regulators.

Similar deduction can be made considering the unbalance and distortion suppression in grid current output. Based on (11), Fig. 7 shows the similar Bode diagram of GSC and L filter impedance regarding unbalance and distortion suppression using R and VPI regulators. The similar conclusions as Fig. 6 can be obtained, thus for the sake of simplicity, they will not be described in detail here.

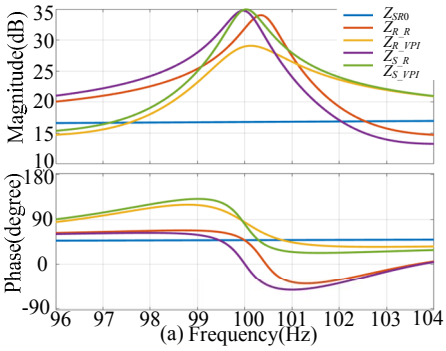

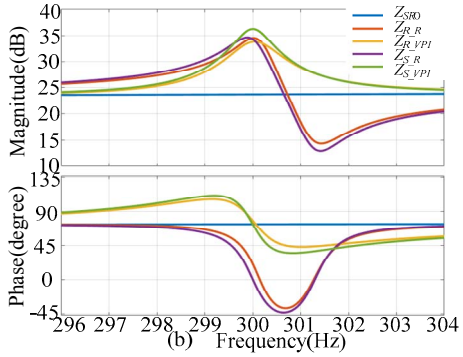

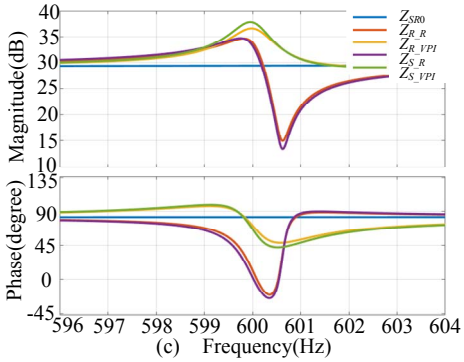

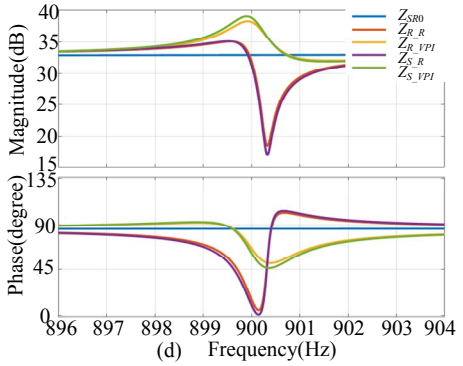

Fig. 6. Bode diagram of DFIG and RSC impedance, using indirect rotor current control and direct stator current control, with R and VPI regulator, k_r = 50, ω_c=5 rad/s, ω_0=100π rad/s, (a) unbalance suppression, k_{pr} = 0.079, n=2; (b) 5th and 7th distortion suppression, k_{pr} = 0.026, n=6; (c) 11th and 13th distortion suppression, k_{pr} = 0.013, n=12; (d) 17th and 19th distortion suppression, k_{pr} = 0.009, n=18;

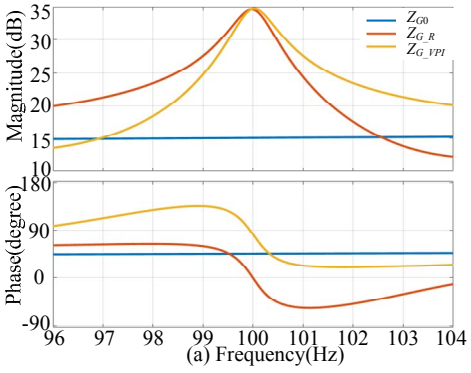

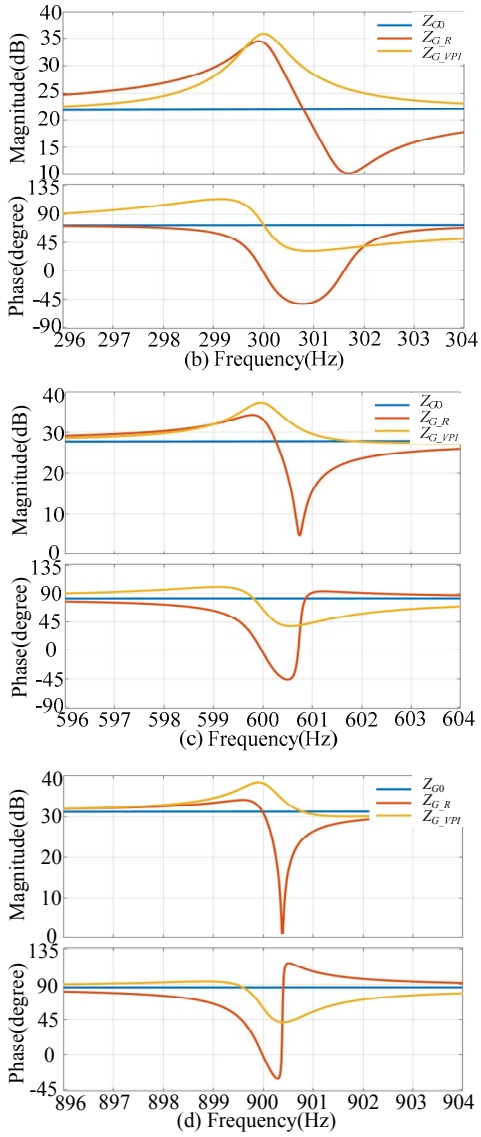

Fig. 7. Bode diagram of GSC and L filter impedance, using grid current control, with R and VPI regulator, k_r = 50, ω_c=5 rad/s, ω_0=100π rad/s, (a) unbalance suppression, k_{pr} = 0.079, n = 2; (b) 5th and 7th distortion suppression, k_{pr} = 0.026, n = 6; (c) 11th and 13th distortion suppression, k_{pr} = 0.013, n = 12; (d) 17th and 19th distortion suppression, k_{pr} = 0.009, n =18;

IV. Simulation Validation

In order to better validate the above analysis and comparison, the MATLAB/Simulink is employed to conduct the simulation validation. The parameters of the simulated 7.5 kW DFIG system can be found in Table II. Due to the limited space, the suppression of harmonic sequence 17th and 19th is simulated as an example.

TABLE II. Parameters of the DFIG System

L_g	11 mH	$L_{\sigma s}$	3.44 mH	R_s	0.44 Ω	R_r	0.64 Ω
T_d	1.5e-4 s	L_m	79.3 mH	K_{prsc}	4	K_{irsc}	12
f_s/f_{sw}	10/5 kHz	$L_{\sigma r}$	5.16 mH	K_{pgsc}	4	K_{igsc}	12

TABLE III. Simulation Results Analysis Data

	No regulator	R regulator	VPI regulator
Stator Current	17^{th} 8.9% 19^{th} 9.6%	17^{th} 8.2% 19^{th} 8.9%	17^{th} 2.3% 19^{th} 2.7%
Grid Current	17^{th} 16.5% 19^{th} 18.7%	17^{th} 15.2% 19^{th} 15.6%	17^{th} 5.8% 19^{th} 6.7%

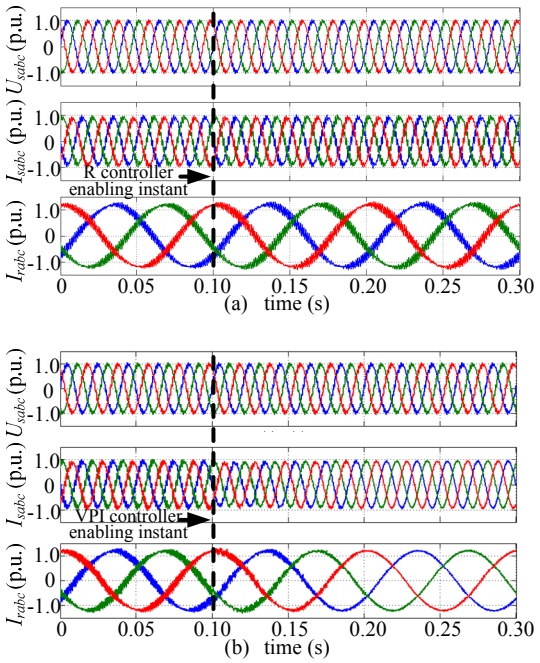

Fig. 8. Simulation result of DFIG stator output current (a) with R controller enabling instant response; (b) with VPI controller enabling instant response;

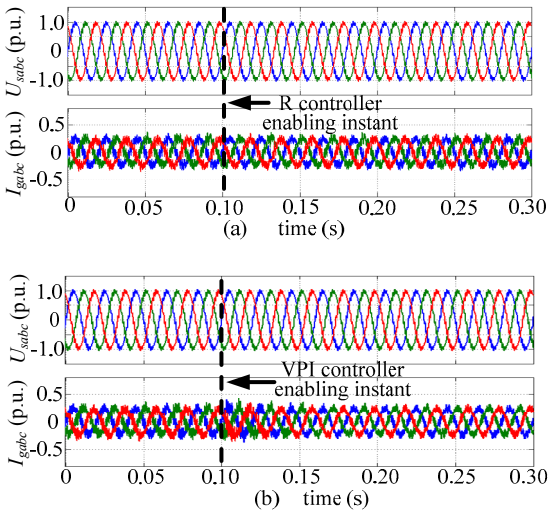

Fig. 9. Simulation result of DFIG grid side output current (a) with R controller enabling instant response; (b) with VPI controller enabling instant response;

Fig. 8 shows the simulation results of DFIG stator output current (a) with R controller enabling instant response; (b) with VPI controller enabling instant at time = 0.1s. When the R controller is enabled, the stator current contains 17th and 19th high order harmonic distortions both before and after the enabling instant, since no effective magnitude increase can be obtained as shown in Fig. 6(d). On the other hand, when the VPI controller is enabled, the stator current 17th and 19th harmonic sequence can be successfully mitigated due to the virtual impedance of positive inductance + positive resistance. The simulation results are able to validate the correctness of the above analysis. Similar conclusion considering GSC output current can be obtained based on the simulation results in Fig. 9, i.e., the VPI controller is able to mitigate the higher order harmonic sequences, while the R controller fails to eliminate the

output current distortion. The simulation result analysis data are available in Table III.

V. Conclusion

This paper has investigated the DFIG system output current unbalance and distortion suppression using the R and VPI controller based on the impedance modeling method. Due to the inevitable digital control delay, the introduction of R controller is equivalent to the insertion of virtual negative inductor and virtual positive resistor, while the introduction of VPI controller is equivalent to the insertion of virtual positive inductor and virtual positive resistor. As a consequence, the VPI has the advantageous performance over R controller, i.e., better suppression of the output current unbalance and distortion.

References

[1] J. Hu, H. Xu, and Y. He, "Coordinated Control of DFIG's RSC and GSC Under Generalized Unbalanced and Distorted Grid Voltage Conditions," *IEEE Trans. Ind. Electron*., vol. 60, no. 7, pp. 2808-2819, July 2013.

[2] H. Xu, J. Hu, and Y. He, "Integrated Modeling and Enhanced Control of DFIG Under Unbalanced and Distorted Grid Voltage Conditions," *IEEE Trans. Energy Convers*., vol. 27, no. 3, pp. 725-736, July 2012.

[3] J. Hu, Y. He, L. Xu, and B.W. Williams, "Improved Control of DFIG Systems During Network Unbalance Using PI–R Current Regulators," *IEEE Trans. Ind. Electron.*, vol. 56, no. 2, pp. 439-451, Feb. 2009.

[4] J. Hu, H. Nian, H. Xu, and Y. He, "Dynamic Modeling and Improved Control of DFIG under Distorted Grid Voltage Conditions," *IEEE Trans. Energy Convers.*, vol. 26, no. 1, pp. 163-175, March 2011.

[5] H. Xu, J. Hu, and Y. He, "Operation of Wind-Turbine-Driven DFIG Systems Under Distorted Grid Voltage Conditions: Analysis and Experimental Validations," *IEEE Trans. Power Electron.*, vol. 27, no. 5, pp. 2354-2366, May 2012.

[6] C. Liu, F. Blaabjerg, W. Chen, and D. Xu, "Stator Current Harmonic Control With Resonant Controller for Doubly Fed Induction Generator," *IEEE Trans. Power Electron*., vol. 27, no. 7, pp. 3207-3220, July 2012.

[7] Y. Song, H. Nian, "Modularized Control Strategy and Performance Analysis of DFIG System Under Unbalanced and Harmonic Grid Voltage," *IEEE Trans. Power Electron.*, vol. 30, no. 9, pp. 4831 - 4842, Sept. 2015.

[8] X. Wang, F. Blaabjerg, and Z. Chen, "Synthesis of Variable Harmonic Impedance in Inverter-Interfaced Distributed Generation Unit for Harmonic Damping Throughout a Distribution Network," *IEEE Trans. Ind. Appl*., vol. 48, no. 4, pp. 1407-1417, July-Aug. 2012.

[9] I. Vieto, and J. Sun, "Impedance modeling of doubly-fed induction generators," *in Proc. Power Electronics and Applications (EPE'15 ECCE-Europe)*, pp. 1-10, Sep. 2015.

[10] I. Vieto, and J. Sun, "Damping of Subsynchronous Resonance Involving Type-III Wind Turbines," *in Proc. Control and Modeling for Power Electronics (COMPEL)*, pp. 1-8, 2015.

[11] I. Vieto, and J. Sun, "Small-Signal Impedance Modelling of Type-III Wind Turbine," *in Proc. Power & Energy Society General Meeting (PESG)*, pp. 1-5, 2015.

[12] I. Vieto, and J. Sun, "Real-time simulation of subsynchronous resonance in Type-III wind turbines," *in Proc. Control and Modeling for Power Electronics (COMPEL)*, pp. 1-8, 2014

[13] Z. Miao, "Impedance-Model-Based SSR Analysis for Type 3 Wind Generator and Series-Compensated Network," *IEEE Trans. Energy Convers.*, vol. 27, no. 4, pp. 984–991, Dec. 2012.

[14] L. Piyasinghe, Z. Miao, J. Khazaei, and L. Fan, "Impedance Model-Based SSR Analysis for TCSC Compensated Type-3 Wind Energy Delivery Systems," *IEEE Trans. Sustainable Energy*., vol. 6, no. 1, pp. 179–187, Jan. 2015.

[15] L. Fan, and Z. Miao, "Nyquist-Stability-Criterion-Based SSR Explanation for Type-3 Wind Generators," *IEEE Trans. Energy Convers.*, vol. 27, no. 3, pp. 807–809, Sep. 2012.

[16] L. Fan, and Z. Miao, "Mitigating SSR Using DFIG-Based Wind Generation," *IEEE Trans. Sustainable Energy.*, vol. 3, no. 3, pp. 349–358, July 2012.